Observations and modeling of San Diego beaches during El Niño

André Doria[1], R.T. Guza[1], William C. O'Reilly[1], and M.L. Yates[2,3]

[1]Scripps Institution of Oceanography, La Jolla, California

[2]Saint-Venant Hydraulics Laboratory, Université Paris-Est (ENPC, EDF R&D, Cerema), Chatou, France

[3]Cerema

Corresponding author address: R.T. Guza, Scripps Institution of Oceanography, 9500 Gilman Drive, La Jolla, CA 92093. E-mail rguza@ucsd.edu

KEY POINTS

1) Subaerial sand levels were observed at 5 southern California beaches for 16 years.

2) Cobbles and bedrock sometimes reduced the mobility of eroded shorelines.

3) Inclusion of site-specific geological boundaries improves the performance of an equilibrium model.

Abstract: Subaerial sand levels were observed at five southern California beaches for 16 years, including notable El Niños in 1997-98 and 2009-10. An existing, empirical shoreline equilibrium model, driven with wave conditions estimated using a regional buoy network, simulates well the seasonal changes in subaerial beach width (e.g. the cross-shore location of the MSL contour) during non-El Niño years, similar to previous results with a 5-year time series lacking an El Nino winter. The existing model correctly identifies the 1997-98 El Niño winter conditions as more erosive than 2009-10, but overestimates shoreline erosion during both El Niños. The good skill of the existing equilibrium models in typical conditions does not necessarily extrapolate to extreme erosion on these beaches where a few meters thick sand layer often overlies more resistant layers. The modest over-prediction of the 2009-10 El Niño is reduced by gradually decreasing the model mobility of highly eroded shorelines (simulating cobbles, kelp wrack, shell hash, or other stabilizing layers). Over prediction during the more severe 1997-98 El Niño is corrected by stopping model erosion when resilient surfaces (identified with aerial imagery) are reached. The trained model provides a computationally simple (e.g. nonlinear first order differential equation) representation of the observed relationship between incident waves and shoreline change.

1. Introduction

Coastal communities and beaches provide abundant ecological, recreational, and socio-economic wealth [*Nicholls et al.*, 2007; *Yang et al.*, 2012; *McLachlan and Brown*, 2010]. Increasing coastal populations [*Moore et al.*, 1999], long-term climate change [*Keeling et al.*, 1995; *Rahmstorf et al.*, 2007], polar ice melt [*Dyurgerov and Meier*, 2000; *Bamber et al.*, 2009], and sea level rise (SLR) forecasts of between 0.8-2 m of SLR by 2100 have raised concerns about the long-term (e.g. centuries) fate of beaches, coastal infrastructure, and coastal cliff retreat [*Zhang et al.*, 2004, *Pfeffer et al.*, 2008; *Vermeer and Rahmstorf*, 2009; *Gallien et al.*, 2011]. At shorter time scales, accelerated coastal erosion may be caused by decadal oscillations in the frequency, severity, and tracks of storms [*Graham and Diaz*, 2001; *Allan and Komar*, 2006 & 2002; *Ruggiero et al.*, 2010a]. California, Oregon, and Washington beaches suffered severe erosion from the intense and frequent storms during the El Niños of 1997-98 and 2009-10 [*Revell et al.*, 2002, 2011; *Barnard et al.*, 2011].

Effectively managing beaches now, and in a future with potentially altered wave climates, requires quantifying the relationship between beach change and waves. However, testing of shoreline change models on the U.S. West coast has been limited. Genres of shoreline models include process-based and empirical. Process models [e.g. SBEACH, *Larson and Kraus*, 1989; XBeach, *Roelvink et al.*, 2009; and CSHORE, *Johnson et al.*, 2012] necessarily parameterize the complex physics of sediment transport with combined steady and oscillatory flows. Empirical models based on an equilibrium hypothesis tune "bulk response" parameters, and have skill in simulating observations of shoreline change on time scales of months to a few years [*Miller and Dean*, 2004; *Yates*

59 *et al.*, 2009a; *Davidson et al.*, 2010, *Ruggiero et al.*, 2010b, *Davidson et al.*, 2013;
60 *Splinter et al.*, 2014]. Equilibrium beach models quantify the hypotheses [*Wright et al.*,
61 1985] that: (a) for a constant wave field, there is an equilibrium beach morphology (the
62 equilibrium beach) that would remain constant in time, neither eroding or accreting, (b) a
63 beach in disequilibrium with the ambient waves changes towards the equilibrium shape,
64 and (c) the change rate is proportional to the disequilibrium. *Miller and Dean* [2004]
65 applied equilibrium concepts to derive

66 $$\frac{dS}{dt} = k(S_{eq}(t) - S(t)) \quad (1)$$

67 where S is the shoreline location (defined as the cross-shore position of a shallow depth
68 contour, here Mean Sea Level (MSL)), $S_{eq}(t) - S(t)$ is the beach disequilibrium, and the
69 empirical k depends on wave energy, grain size, and other local factors. *Yates et al.*
70 [2009a] (hereafter *Y09*) showed that an equilibrium shoreline model had skill at three
71 southern California beaches over five years (2004-2009). *Ludka et al*. [2015] recently
72 developed an equilibrium beach profile model using up to 10 years of observations that
73 included the 2010 El Niño. Here, the southern California observations of previous studies
74 [*Shepard*, 1950, *Winant et al.*, 1975; *Nordstrom and Inman*, 1975; *Flick and Waldorf*,
75 1984, *Yates et al.*, 2009a, 2009b, 2009c] are expanded to include additional sources
76 spanning up to 16 years (1997-2014), including the more severe 1997-98 El Niño winter.
77 The *Y09* shoreline model is extended by gradually decreasing the model mobility of
78 highly eroded shorelines (coarsely accounting for cobbles and other natural armoring),
79 and stopping erosion when a non-erodible layers (e.g. bedrock) is reached.

First, the beach sites (Section 2), and wave and sand level observations (Section 3) are described. In Section 4, observations of waves and shoreline (MSL contour) location are used to tune an equilibrium-type shoreline model. Results are discussed in Section 5, and summarized in Section 6.

2. Beach Sites

In southern California, wave conditions and beach sand levels vary seasonally [*Shepard*, 1950, *Winant et al.*, 1975; *Nordstrom and Inman*, 1975; *Flick and Waldorf*, 1984, *Yates et al.*, 2009a, 2009b, 2009c]. Sand elevations were measured at five San Diego County beaches (from south to north, Figure 1): Imperial Beach (4 km alongshore span), Torrey Pines (8 km), Solana Beach (2.6 km), Cardiff (2 km), and Camp Pendleton (2.5 km). Median sand sizes range between 0.15-0.28 mm (Table 1), and beach slope between 0.01-0.08 (Table 1).

Imperial Beach (Figure 1b) contains a recreational pier, two short groynes in the northern 300 m, and the Tijuana River mouth at the southern end. Most of the beach is backed by low-lying urban development and protective riprap, seawalls, and cobble berms (Figure 2). The southern 6.5 km of Torrey Pines State Beach (Figure 1c), is backed by 50-110 m high-relief sandstone cliffs, and the northern 1.5 km is fringed by riprap and the Los Peñasquitos Lagoon inlet [*Moore et al.*, 1999; *Young et al.*, 2010]. Solana Beach (Figure 1d) is backed by 25 m sandstone cliffs [*Young et al.*, 2010] often armored with seawalls and gunite. Cardiff (Figure 1d) is a straight, narrow beach that extends 2 km north from Solana Beach to the San Elijo Lagoon inlet. Riprap and public parking lots

102 border the back beach. A 200 m long cobble berm, near the upper swash limit, is located
103 at the southern end of the Cardiff site. The Camp Pendleton site (Figure 1b) spans 2.5 km
104 north from the Santa Margarita River outlet, and the beach is backed by a vegetated low
105 dune. During energetic winter waves, foreshore cobble patches (10s of meters in lateral
106 extent) can be exposed at all beaches except Camp Pendleton, which is sandy year-round.

107 Digital orthographic and non-orthographic imagery was used to characterize the
108 back beach type (e.g. seawall, hard cliff, soft dune, rip-rap, none) and the exposed beach
109 face substrates (e.g. bedrock, cobbles, mixed, unknown) during the El Niño 2010 winter
110 (Figure 2). The non-orthographic aerial imagery (Figure 2b) was collected near the 2010
111 El Niño maximum erosion (e.g. February 1-2, 2010) during low tide from a U.S. Coast
112 Guard helicopter with a high-resolution DSLR camera. Orthographic aerial imagery was
113 collected by Fugro EarthData, Inc. from 26 August - 29 November, 2010 using an
114 airborne orthographic imaging system (Leica ADS40-SH52) with 2 m horizontal
115 accuracy and 30 cm pixel resolution.

116 The non-orthographic 2010 winter aerial imagery was visually referenced to the
117 orthographic imagery to estimate the horizontal locations of subaerial beach substrates
118 exposed during El Niño 2010 erosion (colored polygons in Figure 2a). Non-erodible
119 surfaces above the sand level included boulders, rock outcroppings and ledges, cobble
120 berms and low relief bedrock. Features visible in 2010 above MSL (e.g. the cobbles in
121 Figure 2b are above MSL) were assumed to continue below sand level at a steep, near-
122 vertical slope. Low relief features exposed in 1997-98 may not have been detected in
123 2009-10.

124 The vertical elevations of exposed non-erodible surfaces were then estimated

from the airborne lidar survey (February 26, 2010) occurring 24 days after the USGC aerial photo survey. Lidar and imagery based estimates of the subaerial substrate locations and types agreed qualitatively with ATV substrate surveys collected at all sites within 9 days of the aerial photo survey. Comparable detailed mapping was not available for the 1997-98 El Niño.

3. Observations

3.1. Sand Level Surveys

Surveys of subaerial beach sand levels from 1997-2014 at 5 beaches were obtained from several sources (Figure 1) including (1) cross-shore transects surveyed biannually from the back beach to ~8-10 m depth beginning in 1997 (San Diego Association of Governments (SANDAG); red transects in Figure 1) and (2) quarterly transects, beginning in 2004 (SIO; dense black, blue, or white transects in Figure 1) [*Yates et al.*, 2009a]. (3) Monthly subaerial shoreline parallel surveys beginning at Torrey Pines, and subsequently expanded to four additional sites (Imperial, Cardiff, Solana, and Camp Pendleton). (4) Airborne lidar in April 1998 (NASA's airborne topographic mapper (ATM); *Brock et al.*, [2002]) and biannually from May 2002 until October 2010 (Univ. of Texas, *Yates et al.*, [2008]). Lidar returns were removed offshore of the waterline location, estimated using water levels from a nearby tide gauge and runup approximated using local wave conditions [*Yates et al.*, 2008]. Lidar sand levels were gridded onto 4 m^2 cells, using the cell median elevation to reduce the influence of outliers. Point density in the 1998 NASA lidar survey was low (0.57 points m^{-2}), compared with the post-2001 biannual lidar surveys (~2 points m^{-2}) [*Brock et al.*, 2002;

148 *Yates et al.*, 2008]. Grid cells with less than 3 data points were discarded from the post-
149 2001 lidar surveys. All data was necessarily retained in the lower density 1998 survey.
150 Surveys from different sources at the same approximate time and beach usually agree,
151 with differences owing to variable amounts of spatial averaging (Figure 3).

152 Responding to seasonal variations in wave energy, the observed shoreline (e.g. MSL
153 contour) locations usually varied seasonally by 25-30 m at all 5 study beaches (Figure 4;
154 [*Winant et al.*, 1975; *Yates et al.*, 2009b]). During the 1998 El Niño, shoreline retreat was
155 maximal, about 25 m landward of the typical (e.g. 2004-2012) winter shoreline (Figure
156 4). Recovery from 1997-98 took several years, even with nourishments both shortly
157 before (1997, Imperial Beach, 178,000 m^3) and after (1999, Solana Beach, 41,000 m^3) El
158 Niño; however, during fall 1997, existing beach sand levels at several sites were
159 historically lower than post-summer level observed in most other years. Accordingly, the
160 erosive change during the 1997-98 El Niño was limited because of low sand levels
161 preceding the event. Recovery following the less erosive 2009-10 El Niño was more
162 rapid, effectively one season (Figures 3 and 4). Spring-summer 2001 nourishments at
163 Imperial Beach, Torrey Pines, Solana Beach, and Cardiff elevated sand levels to new
164 maxima (Figure 4). The nourishment was detectable for about two years at Torrey Pines,
165 either as a wider subaerial beach, or as an enhanced offshore winter sand bar [*Yates et al.*,
166 2009c]. SANDAG winter surveys occur in spring and fall. The spring surveys usually
167 occur after the winter erosion maximum in February-March (compare squares and circles
168 in Figure 3a, in 2005-2008 inclusive), so the 1998 survey may not have captured the
169 maximum erosion.

170

3.2. Waves

Waves typically approach the Southern California Bight from N-NW in winter and from S-SW in summer, and vary alongshore owing to sheltering by the Channel Islands and refraction over complex offshore bathymetry [*Pawka*,1983]. Local (e.g. < 30 m depth) bathymetric variations further refract and focus waves with appreciable alongshore energy variations over several hundreds meters alongshore. Directional wave buoys (CDIP, http://cdip.ucsd.edu; Figure 1a) initialized a spectral refraction model [*O'Reilly and Guza*, 1991, 1993, 1998] that provided hourly wave estimates at 10 m depth every 100 m alongshore. Near-shore buoy deployments confirmed reasonably good model accuracy in relatively shallow water (20-30 m depth) at several of the study sites [*Young et al., 2012*].

Waves were most energetic during strong El Niño winters (Figure 5a). For example, at the Oceanside buoy (Figure 1b), the hours of significant wave height H_s exceeding 3 m were between 0-26 hours during 13 non-El Niño winters, compared with 40 and 51 hours in the 1997-98 and 2009-10 El Niño winters, respectively. Total hours of H_s between 2-3 m during the 1997-98 El Niño winter (more than 400 hours) dwarfed all other winters, nearly doubling those found in the second most energetic winter (e.g. 2009-10 winter; 220 hours of H_s = 2-3 m; Figure 5a). In 1997-98, H_s exceeded 2 m for nearly 60 continuous hours, with frequent and prolonged sequences of energetic waves in early December 1997 and February 1998 (Figure 5b). January 2010 had the longest period (~ 140 hours) of continuous H_s exceeding 2 m (Figure 5e).

4. Shoreline Modeling

193 **4.1. Equilibrium Shoreline Model**

194 An existing equilibrium shoreline model [*Y09*] was modified to improve
195 predictions during El Niños and other severe erosion conditions by accounting for
196 durable limits (e.g. bedrock, seawalls, hard cliffs). The model assumes these relatively
197 resilient boundaries were not eroded during the modeling period, and neglects cliff
198 erosion, which would both relocate the back beach boundary and supply new sand to the
199 beach. The comparative beach profile effects between armored and exposed back beaches
200 are not included in the present model. With the shoreline location S defined as the cross-
201 shore location of the MSL contour, the shoreline change rate dS/dt depends on the
202 present shoreline position S and incident wave energy E,

203 $$\frac{dS}{dt} = \begin{cases} C^{\pm} E^{1/2} \Delta E(S) & \text{for } S > S_{bb} \\ 0 & \text{for } S \le S_{bb} \end{cases} \quad \text{(2a)}$$

204 where $C^{\pm}$ are two change rate coefficients for accretion (C^{+}) and erosion (C^{-}), and the
205 wave energy disequilibrium is

206 $$\Delta E(S) = E - E_{eq}(S). \quad \text{(2b)}$$

207 E_{eq}, the equilibrium wave energy, is the wave energy for a given S that would cause no
208 shoreline change . For the few occasions when highly accreted shoreline positions S^{+}
209 yielded non-physical negative E_{eq} (e.g. $E_{eq}(S^{+}) < 0$), $E_{eq}(S^{+}) \equiv 0$, ensuring non-
210 negative equilibrium wave energy. Unless otherwise noted, E_{eq} is linearly related to the
211 shoreline position S:

$$E_{eq}(S) = a_0 + a_1 S \quad (3)$$

where a_0 and a_1 are empirically determined equilibrium wave energy coefficients. New here, S_{bb} is the non-erodible back beach cross-shore location defined using the aerial photographic and lidar surveys. Shoreline retreat stops (e.g. $dS/dt = 0$) when $S = S_{bb}$. A beach initially in equilibrium and subject to a step change in the incident wave energy equilibrates exponentially, with a characteristic e-folding time scale $\tau^{\pm} = \left| a_1 C^{\pm} \sqrt{E} \right|^{-1}$ [*Y09*].

Each beach was sub-divided into approximately 500 m alongshore sections, numbered from south to north within each site: I1-I9 (Imperial Beach), T1-T9 (Torrey Pines), S1-S5 (Solana Beach), C1-C4 (Cardiff), P1-P4 (Camp Pendleton). Incident wave energy, temporally-demeaned shoreline observations, and the back beach limit S_{bb} (Figure 2) were alongshore averaged on transects within each 500 m section. Values of the model's four free parameters (C^+, C^-, a_0, a_1) were determined from these averaged shoreline observations and hourly wave estimates by minimizing the model-data root-mean-square error (RMSE) using surrogate management framework (SMF) optimization [*Booker et al.*, 1999; *Marsden et al.*, 2004].

4.2. Model-Data Comparison

Shorelines were hindcast for up to 16 years using the wave-driven equilibrium model, initialized with the earliest survey data point (typically fall 1997). Model calibration with a period including an El Niño yielded improved model-data agreement during both El Niño and non-El Niño years, and calibration with 2003-2011 is shown

233 (Figure 6). The average model skill at Solana, Imperial and Torrey Pines beaches are
234 between 0.55-0.60 (Table 3). At Cardiff and Camp Pendleton, two shorter beaches with
235 river or lagoon mouths, skill was often less than 0.5. Two of the four modeled sections at
236 Cardiff have low skill (e.g. 0.22 and 0.41) and are located near a persistent lagoon mouth
237 or a large bedrock platform extending from the subearial beach to wading depths. Camp
238 Pendleton was observed for the shortest time, and has the lowest R^2 (less than 0.5 at all
239 modeled sections; Figure 6e), possibly resulting from the adjacent river mouth. Skill at all
240 modeled locations was significant at the 95% level.

241 The model back beach erosive limit S_{bb} (Figure 2; dashed horizontal line in
242 Figure 6a-d) was reached during the 1997-98 El Niño (except Camp Pendleton), and
243 without the geological constraint the unmodified *Y09* model over-predicted erosion (red
244 curve in Figure 6). S_{bb} was reached only at a few sites in the 2009-10 El Niño. The
245 maximum model beach width $S_{\max} = -a_0/a_1$ (positive horizontal dotted line in Figure 6)
246 was exceeded a few times, usually after sand nourishments that are neglected in the
247 model (e.g. accretion peaks in fall 1998 and fall 2001 at Imperial Beach (Figure 6a) and
248 during summer-fall 2001 at Torrey Pines and Solana Beach (Figure 6b,c)). The
249 anomalous accretive peak in summer 2006 at many of the sites is unexplained and not
250 reproduced by the model.

251 **5. Discussion**

252 **5.1. Parameter Values, Response Times, and Initialization**

253 Optimal model free parameters varied within and between sites (Table 3). Model

error is weakly sensitive to the free parameter values, with only a 10% increase in model error for factor of two of changes in parameters (comparable to the differences between sites). Free parameter values surely depend on sediment availability, grain size, and possibly other environmental factors, but are only loosely constrained by the observations.

The best-fit shoreline adjustment time scales $\tau^{\pm} = \left| a_1 C^{\pm} \sqrt{E} \right|^{-1}$, averaged over each site, varied between roughly 10-20 days for erosion τ^{-} (with $H_s = 4$ m), and the accretion τ^{+} spanned 29-64 days (with $H_s = 1$m; Table 3). Hypothetical initial conditions illustrate the rapid return (weeks to several months) of the model to equilibrium from artificially large disequilibria (crosses and triangular markers in Figure 7). Six rather different initial conditions in 1996, 1997, and 1998 all result in the same modeled shoreline by summer 1998 (grey curve in Figure 7). Model shorelines recovered from strong 1997-98 El Niño erosion by the following winter, more rapid than the observed multi-year recovery, demonstrating the model's failure to properly replicate the slow return of sand evidently displaced further offshore during the strong event (Figures 6b-d). Accretion is crudely parameterized in the model and requires future study.

5.2. Calibration Period

At Torrey Pines, *Y09* found a relative 1.9 m increase in model-data RMSE during predictive model periods compared to the calibration period RMSE. *Splinter et al.* [2013] provide a more extensive calibration and validation discussion of a similar equilibrium-based 1-D shoreline model. Both Y09 and *Splinter et al.* [2013] showed that

approximately two years of monthly observations suffice to calibrate empirical shoreline model parameters on seasonally variable beaches (Torrey Pines in southern California and along the eastern Australian coast). Here, three calibration periods are examined (Figure 8): 1997-2013 (all data; 16 years), 2003-2011 (8 years), and 2003-2008 (5 years). The 2003-2008 period lacks an El Niño. Model errors are characterized with the RMSE over 16 years, and with Δ_{W10}, the difference between the maximum erosion observed and modeled during the 2009-10 El Niño winter. Solana Beach results weakly depended on calibration period (Figure 8, top). At the other sites, longer calibration periods that included an El Niño consistently decreased Δ_{W10} and RSME over the entire 16-year observation period, which included years of neutral and La Niña conditions (Figure 9a,b). The sparse 1997-2001 data were not well fit, even when 1997-2001 was included in the calibration (not shown). The 2003-2011 calibration period was used.

The alongshore variability of the 8-year calibration model coefficients was qualitatively similar to previous work [*Y09*] based on ~5 years of calibration that did not include El Niño (similar to the 2003-2008 calibration results in this study). Here, the relative magnitudes of the wave energy slope, a_1, and $C^{\pm}$ were reversed compared to *Y09* (e.g. *Y09* had larger (smaller) magnitude a_1 ($C^{\pm}$) compared to this study). These differences may be partially attributed to the increased calibration period, as longer tuning generally resulted in different free parameters and a reduction in RMSE [*Y09*]. However, direct comparison to the *Y09* results is cautioned, as modeled sections at the same beach are not necessarily identical to this study.

Additionally, the statistical nature of the calibration technique creates inherent

297 variation to the resulting coefficients, as several solutions in parameter-space may
298 produce similar results. The multiplicative nature of the model terms (2) also allows for
299 changes in one coefficient to be compensated for by another coefficient.

300 Alongshore-averaged model coefficients provide a broad representation of the
301 site-specific free-parameter value for bulk comparison to *Y09* (Table 3). Alongshore
302 averaged, C^+ had the greatest disparity (more than double in magnitude) relative to *Y09*
303 5-year calibrated C^+ at Torrey Pines. However, as noted previously, model skill is fairly
304 insensitive to parameter values, with C^+ being the least sensitive parameter [*Y09*].
305 Fundamentally, model coefficients are weakly constrained by observations and
306 differences between studies, even at similar beaches, are not necessarily remarkable.

307 **5.3. Alternative Model Formulations**

308 *Davidson et al.* [2013] and *Splinter et al.* [2014] use an equilibrium model with
309 forcing governed by wave power (rather than wave energy, E, in (2)) and the Dean
310 parameter, which depends on grain size. The range of sand grain sizes is not taken into
311 account here, and is relatively small (4 of the 5 beaches have D_{50} between 0.15-0.18mm,
312 (Table 1)). At Torrey Pines, *Y09* showed replacing wave energy, E, in their shoreline
313 model with H_s or radiation stress S_{xx} resulted in similar model skill, because E, H_s, and
314 S_{xx} are strongly mutually correlated. *Davidson et al.* [2013] and others use an equilibrium
315 condition based on the weighted average of antecedent waves, rather than on the present
316 beach state. However, the present beach state depends on the previous wave conditions,
317 and for the idealized case of a step change in time to a constant wave forcing, the
318 equilibrium conditions of *Davidson et al.* [2013] and *Y09* yield identical results. These

319 different equilibrium models were also shown to yield similar results for the field
320 observations [*Castelle et al.*, 2014].

321 The basic equilibrium equation of the present model (2), with a linear dependence
322 of dS/dt on the present wave energy E, and 4 free parameters, is referred to as the
323 linear$_4$ model (the subscript specifies the number of free parameters). Additional
324 alternative models are linear$_3$, exp$_4$, and cubic$_4$. The linear$_3$ model reduces the number of
325 free parameters to three by replacing $C^{\pm}$ with single valued C in (2a), following *Yates*
326 *et al.*, [2011]. The exp$_4$ and cubic$_4$ alternative models also simplify $C^{\pm}$ with C in (2a),
327 but use more complex forms of E_{eq},

328 $$E_{eq} = a_0 e^{a_1(S-a_2)} \quad \text{for exp}_4 \tag{4}$$

329 and

330 $$E_{eq} = a_0 + a_1 S + a_2 S^3 \quad \text{for cubic}_4. \tag{5}$$

331 The model parameters S_{eq} and E_{eq}, and the rate of change dS/dt and the response time
332 τ, are similar in the range of common S and H_s, while differing at the extremes (Figure
333 10). All models use the same erosion limiter S_{bb}.

334 Overall (2003-2011) the alternative models perform similarly, with typically
335 small (<15%) improvements in model error relative to the *Y09* model, which has no
336 erosion limiter (Figure 9c). Model performance varied by site, but explained more than
337 50% of the variance over 16 years at most of the sandy beaches, similar to *Y09* five-year
338 hindcasts. The models differ from the *Y09* model most significantly for extreme

conditions only briefly encountered. While the *Y09* model correctly identifies the 1997-98 waves as more erosive than 2009-10, it overestimates shoreline erosion during both El Niño events.

The cubic$_4$ model provided the greatest improvements in model skill (relative to *Y09*), with improved predictions for El Niño 2009-10 at beaches both where the erosion limiter was and was not reached (Solana Beach and Torrey Pines, respectively, Figure 9a,b). The over-prediction of the winter 2009-10 shoreline erosion (Δ_{W10}, Figure 9d) was reduced using the cubic$_4$ model at all sites except Camp Pendleton, where over-prediction persisted. Model-data comparison at Camp Pendleton was generally poor irrespective of which model was used, perhaps owing to the close proximity of a river mouth. Typical Δ_{W10} reductions are about 5 m (up to 18 m peak reduction) relative to *Y09*. With large waves (H_s = 4 m) and a heavily eroded shoreline (solid curves, S = -40 m, Figure 10d), dS/dt for exp$_4$ and cubic$_4$ are much smaller in magnitude than for linear$_3$ (a simplified version of the *Y09* model). Physical explanations for the reduced mobility of eroded beach face include the exposure of resistant strata and/or a reduction of the effective wave energy reaching the beach face owing to well-developed offshore sandbars.

6. Conclusion

Sixteen years of shoreline and wave observations, including two El Niños, 1997-98 and 2009-10, illustrate seasonal and long-term fluctuations in wave climate and shoreline sand levels at five southern California beaches. An existing, empirical shoreline model driven with hourly wave conditions simulates well the seasonal changes in subaerial beach width (e.g. the cross-shore location of the MSL contour) during non-El

Niño years, similar to previous results [*Y09*]. During El Niño winters the *Y09* model over-prediction of shoreline erosion is reduced by including the location of erosion resistant boundaries (identified with aerial images), and using alternative, nonlinear forms of E_{eq} (e.g. cubic$_4$) that gradually decrease the mobility of highly eroded shorelines (simulating cobbles, kelp wrack, enhanced offshore sand bars, and other stabilizing effects).

The shoreline location depends on complex processes occurring over the cross-shore beach profile, and in some cases on adjacent profiles. Even significantly different equilibrium shoreline models often have similar skill [*Castelle et al.,* 2014], which is also true for existing, more computationally demanding, physical process models for shoreline change. Application of any model to extreme conditions on sand-limited beaches with unknown substrates will requires site and condition specific calibration. Once trained, the present model provides a computationally simple (e.g. nonlinear first order differential equation) representation of the observed relationship between incident waves and shoreline change, including the effect of erosion resistant substrates.

Acknowledgements

This research was supported by the United States Army Corps of Engineers and the California Department of Parks and Recreation Division of Boating and Waterways (program manager Reinhard Flick). The paper was substantially improved by reviewer and editor commments. André Doria was supported by Fellowships from the University of California Regents, NDSEG, and the National Science Foundation (GRFP). SANDAG, Coastal Frontiers Corporation, and Fugro are thanked for their assistance in

using their datasets. This publication was prepared by André Doria under NOAA Grant #NA10OAR4170060. California Sea Grant Project R/RCC-01, through NOAA's National Sea Grant College Program and the U.S. Dept. of Commerce. The statements, findings, conclusions and recommendations are those of the author(s) and do not necessarily reflect the views of the aforementioned organizations.

References

Allan, J. C., and P. D. Komar (2002), Extreme storms on the Pacific Northwest Coast during the 1997–98 El Niño and 1998–99 La Niña, J. Coastal Res., 18(1), 175–193.

Allan, J. C., and P. D. Komar (2006), Climate controls on US West Coast erosion processes, J. Coastal Res., 22(3), 511–529, doi:10.2112/03- 0108.1.

Bamber, Jonathan L., Riccardo E. M. Riva, Bert L. A. Vermeersen, Anne M. LeBrocq (2009), Reassessment of the Potential Sea-Level Rise from a Collapse of the West Antarctic Ice Sheet, Science, 324(5929), 901-903, doi: 10.1126/science.1169335

Barnard, P. L., J. Allan, J. E. Hansen, G. M. Kaminsky, P. Ruggiero, and A. Doria (2011), The impact of the 2009–10 El Niño Modoki on U.S. West Coast beaches, Geophys. Res. Lett., 38(13), doi:10.1029/2011GL047707.

Booker, A. J., J. E. Inman, P. D. Frank, D. B. Serafini, V. Torczon, and M. W. Trosset (1999), A rigorous framework for optimization of expensive functions by surrogates, Struct. Multidiscip. Optim., 17(1), 1–13.

Brock, J.C., C. Wayne Wright, Asbury H. Sallenger, William B. Krabill and Robert N. Swift (2002), Basis and Methods of NASA Airborne Topographic Mapper Lidar Surveys for Coastal Studies, J. Coastal Res., 18(1), 1-13.

California Department of Boating and Waterways and State Coastal Conservancy (2002), California Beach Restoration Study, Sacramento, California Department of Boating and Waterways and State Coastal Conservancy, Sacramento, Cali., http://www.dbw.ca.gov/PDF/Reports/BeachReport/FUll.pdf.

Castelle, Bruno, Vincent Marieu, Stéphane Bujan, Sophie Ferreira, Jean-Paul Parisot, Sylvain Capo, Nadia Sénéchal, and Thomas Chouzenoux (2014), Equilibrium shoreline modelling of a high-energy meso-macrotidal multiple-barred beach, Marine Geology, 347, 85–94, doi:10.1016/j.margeo.2013.11.003.

Coastal Frontiers Corporation (2002), SANDAG 2001 Regional Beach Monitoring Program annual report, Coastal Frontiers Corporation, Chatsworth, Cali., http://www.sandag.org/uploads/projectid/projectid_101_16641.pdf.

426 Davidson, M.A., R.P. Lewis, and I.L. Turner (2010), Forecasting seasonal to multi-year
427 shoreline change, Coastal Engineering, 57(6), 620-629,
428 doi:10.1016/j.coastaleng.2010.02.001.
429
430 Davidson, M.A., K.D. Splinter, and I.L. Turner (2013), A simple equilibrium model for
431 predicting shoreline change, Coastal Engineering, 73, 191–202,
432 doi:10.1016/j.coastaleng.2012.11.002
433
434 Dyurgerov, Mark B., and Mark F. Meier (2000), Twentieth century climate change:
435 Evidence from small glaciers, Proceedings of the National Academy of Sciences, 97(4),
436 1406-1411.
437
438 Flick, Reinhard E., and B.Walton Waldorf (1984), Performance documentation of the
439 Longard Tube at Del Mar, California 1980–1983, Coastal Engineering, 8(3), 199-217,
440 doi:10.1016/0378-3839(84)90001-2.
441
442 Gallien, T.W., J.E. Schubert, and B.F. Sanders (2011), Predicting tidal flooding of
443 urbanized embayments: A modeling framework and data requirements, Coastal
444 Engineering, 58(6), 567-577, doi:10.1016/j.coastaleng.2011.01.011.
445
446 Graham, N. E., and H. F. Diaz (2001), Evidence for intensification of North Pacific
447 winter cyclones since 1948, Bull. Am. Meteorol. Soc., 82, 1869–1893,
448 doi:http://dx.doi.org/10.1175/1520-0477(2001)082<1869:EFIONP>2.3. CO;2.

449

450 Johnson, Bradley D., Nobuhisa Kobayashi, and Mark B. Gravens (2012), Cross-Shore
451 Numerical Model CSHORE for Waves, Currents, Sediment Transport and Beach Profile,
452 ERDC/CHL TR-12-22, Coastal and Hydraulics Lab. (U.S.) Eng. Res. and Dev. Center
453 (U.S.), Vicksburg, Miss.
454
455 Keeling, C. D., T. P. Whorf, M. Wahlen, and J. Van Der Plichtt (1995), Nature, 375, 666-
456 670, doi: 10.1038/375666a0.
457
458 Larson, M., and N. C. Kraus (1989), SBEACH: Numerical model for simulating storm-
459 induced beach change, Tech. Rep. CERC-89-9, U.S. Army Corps of Eng., Vicksburg,
460 Miss.

461

462 Ludka, B. C., R. T. Guza, W. C. O'Reilly, and M. L. Yates (2015), Field Evidence of
463 Beach Profile Evolution Towards Equilibrium, J. Geophys. Res. Oceans, 120,
464 doi:10.1002/2015JC010893.

465

466 Marsden, A. L., M. Wang, J. E. Dennis, and P. Moin (2004), Optimal aerocoustic shape
467 design using the surrogate management framework, Optim. Eng., 5(2), 235–262.
468
469 McLachlan, A., and A. Brown (2010), The Ecology of Sandy Shores, Academic Press,
470 Burlington, Mass.

Miller, Jon K., and Robert G. Dean (2004), A simple new shoreline change model, Coastal Eng., 51(7), 531–556, doi:10.1016/j.coastaleng.2004.05.006.

Moore, L.J., B.T. Benumof, and G. B. Griggs (1999), Coastal erosion hazards in Santa Cruz and San Diego Counties, California, J. Coastal Res., SI(28), 121-139.

Nordstrom, C. E., and D. L. Inman (1975), Sand level changes on Torrey Pines Beach, California, (U.S.) Coastal Eng. Res. Center, Fort Belvoir, Virg.

O'Reilly, W.C. and R.T. Guza (1991), Comparison of spectral refraction and refraction-diffraction wave models, J. Waterway, Port, Coastal, and Ocean Engineering, 117, 199-215.

O'Reilly, W.C., and R.T. Guza (1993), A comparison of spectral wave models in the Southern California Bight, Coastal Eng., 19, 263-282.

O'Reilly, W.C., and R.T. Guza (1998), Assimilating coastal wave observations into regional swell predictions. Part I: Inverse methods, J. Phys. Oceanogr., 28, 679-691.

Pawka, S. S. (1983), Island shadows in wave directional spectra, J. Geophys. Res., 88(C4), 2579–2591, doi:10.1029/JC088iC04p02579.

494 Pfeffer, W. T., J. T. Harper, and S. O'Neel (2008), Kinematic constraints on glacier
495 contributions to 21st- century sea- level rise, Science, 321, 1340–1343,
496 doi:10.1126/science.1159099.

497

498 Rahmstorf, Stefan, Anny Cazenave, John A. Church, James E. Hansen, Ralph F. Keeling,
499 David E. Parker, and Richard C. J. Somerville (2007), Recent Climate Observations
500 Compared to Projections, Science, 316, doi: 10.1126/science.1136843.

501

502 Revell, David L., Paul D. Komar, and Asbury H. Sallenger Jr. (2002), An Application of
503 LIDAR to Analyses of El Niño Erosion in the Netarts Littoral Cell, Oregon, J. Coastal
504 Res., 18(4), 792-801.

505

506 Revell, David L., Jenifer E. Dugan, and David M. Hubbard (2011), Physical and
507 Ecological Responses of Sandy Beaches to the 1997–98 El Niño, J. Coastal Res. 27(4),
508 718 – 730, doi:http://dx.doi.org/10.2112/JCOASTRES-D-09-00179.1.

509

510 Roelvink, Dano, Ad Reniers, Ap van Dongeren, Jaap van Thiel de Vries, Robert McCall,
511 and Jamie Lescinski (2009), Modelling storm impacts on beaches, dunes and barrier
512 islands, Coastal Eng., 56, 1133-1152, doi:10.1016/j.coastaleng.2009.08.006.

513

514 Ruggiero, Peter, P. D. Komar, and J. C. Allan (2010a), Increasing wave heights and

extreme- value projections: The wave climate of the U.S. Pacific Northwest, Coastal Eng., 57, 539–552, doi:10.1016/j.coastaleng. 2009.12.005.

Ruggiero, Peter, Maarten Buijsman, George M. Kaminsky, and Guy Gelfenbaum (2010b), Modeling the effects of wave climate and sediment supply variability on large-scale shoreline change, Marine Geology, 273, 127-140.

Shepard, F.P. (1950), Beach cycles in southern California, Tech. Memo 20, Beach Erosion Board, U.S. Army Corps of Engineers, Washington, D.C.

Splinter, K.D., I. L. Turner, and M. A. Davidson (2013), How much data is enough? The importance of morphological sampling interval and duration for calibration of empirical shoreline models, Coastal Eng., 77, 14-27, doi:10.1016/j.coastaleng.2013.02.009.

Splinter, K. D., I. L. Turner, M. A. Davidson, P. Barnard, B. Castelle, and J. Oltman-Shay (2014), A generalized equilibrium model for predicting daily to interannual shoreline response, J. Geophys. Res., 119, 1936–1958, doi:10.1002/2014JF003106.

Vermeer, M., and S. Rahmstorf (2009), Global sea level linked to global temperature, Proc. Natl. Acad. Sci. U. S. A., 106(51), 21527-21532, doi:10.1073/pnas.0907765106.

Warrick, J.A., K. Rosenberger, A. Lam, J. Ferreira, I. M. Miller, M. Rippy, J. Svejkovsky, and N. Mustain (2012), Observations of coastal sediment dynamics of the Tijuana Estuary Fine Sediment Fate and Transport Demonstration Project, Imperial Beach, California, U.S. Geological Survey, Open-File Report 2012–1083, http://pubs.usgs.gov/of/2012/1083/.

Winant, C. D., D. L. Inman, and C. E. Nordstrom (1975), Description of seasonal beach changes using empirical eigenfunctions, J. Geophys. Res., 80, 1979–1986.

Wright, L.D, A.D Short, and M.O Green (1985), Short-term changes in the morphodynamic states of beaches and surf zones: An empirical predictive model, Marine Geology, 62, 339-364, doi:10.1016/0025-3227(85)90123-9.

Yang, B., M. Madden, J. Kim, and T. R. Jordan (2012), Geospatial analysis of barrier island beach availability to tourists. Tourism Manage., 33, 840–854.

Yates, M.L., R. T. Guza, Roberto Gutierrez, and Richard Seymour (2008), A Technique for Eliminating Water Returns from Lidar Beach Elevation Surveys, J. Atmos. Oceanic Technol., 25, 1671–1682, doi:10.1175/2008JTECHO561.1.

Yates, M. L., R. T. Guza, and W. C. O'Reilly (2009a), Equilibrium shoreline response: Observations and modeling, J. Geophys. Res., 114, doi:10.1029/2009JC005359.

558 Yates, M. L., R. T. Guza, W. C. O'Reilly, and R. J. Seymour (2009b), Overview of
559 seasonal sand level changes on Southern California beaches, Shore & Beach, 77, 39–46.
560
561 Yates, M. L., R. T. Guza, W. C. O'Reilly, and R. J. Seymour (2009c), Seasonal
562 persistence of a small southern California beach fill, Coastal Eng., 56, 559-564,
563 doi:10.1016/j.coastaleng.2008.11.004.
564
565 Yates, M. L., R. T. Guza, W. C. O'Reilly, J.E. Hansen, and P. L. Barnard (2011),
566 Equilibrium shoreline response of a high wave energy beach, J. Geophys. Res., 116, doi:
567 10.1029/2010JC006681.
568
569 Young, A. P., J. H. Raymond, J. Sorenson, E. A. Johnstone, N. W. Driscoll, R. E. Flick,
570 and R. T. Guza (2010), Coarse sediment yields from seacliff erosion in the Oceanside
571 Littoral Cell. Journal of Coastal Research, 26(3), 580–585.
572
573 Young, A. P., R. T. Guza, P. N. Adams, W. C. O'Reilly, and R. E. Flick (2012), Cross-
574 shore decay of cliff top ground motions driven by local ocean swell and infragravity
575 waves, J. Geophys. Res., 117, doi:10.1029/2012JC007908.
576
577 Zhang, Keqi, Bruce C. Douglas, and Stephen P. Leatherman (2004), Global warming and
578 coastal erosion, Climatic Change, 64, 41-58.

Tables

Table 1. Beach Alongshore Distance, Beach Facing Azimuthal Direction, Median Sand Grain Diameter (D_{50}), Beach Slope at MSL, MSL Minimum, Maximum, and Standard Deviation Horizontal Displacement from Average MSL Location, Number of Surveys, and Survey Date Range for Each Site.

Site	Alongshore Distance (km)	Direction (deg)	D_{50} (mm)	Beach Slope	MSL min/max (σ) (m)	Number of Surveys	Date Range
Imperial Beach	4	250-270	0.28[a]	0.02-0.05	-23.6/25.8 (10.5)	97	Oct 1997-Aug 2012
Torrey Pines	8	260-270	0.15[b]	0.01-0.08	-31.5/26.2 (9.1)	226	Oct 1997-Jan 2014
Solana Beach	2.6	240-265	0.15[b]	0.02-0.08	-22.5/20.5 (7.6)	103	Oct 1997-Aug 2012
Cardiff	2	260	0.15[b]	0.02-0.11	-27.3/22.8 (9.5)	136	Oct 1997-Aug 2012
Camp Pendleton	2.5	235	0.18[b]	0.02-0.04	-35.8/19.4 (9.7)	72	Oct 1998-Oct 2010

[a]Collected May 2008 in the swash zone [*Warrick et al.*, 2012].
[b]Collected spring 2006 near the high tide line [*Yates et al.*, 2009b].

Table 2. Historical Beach Nourishment Placement Dates, Receiver Sites, Qualitative Placement Locations, Nourishment Volumes, Nourishment Pad Approximate Length and Width, and Nourishment Sand Median Grain Diameter (D_{50}).

Placement Date	Receiver Site	Placement Location	Volume (10^3 m^3)	Length (m)	Width (m)	D_{50} (mm)
1995	Imperial Beach	Near-shore[a]	31.3	-	-	-
1996	Imperial Beach	Near-shore[a]	35.9	-	-	-
1997	Imperial Beach	Subaerial Beach[b]	13.7	-	-	-
1997	Imperial Beach	Near-shore[a]	178.1	-	-	-
1999	Solana Beach	Subaerial Beach	41.2	-	-	-
6-27 April, 2001	Torrey Pines	Subaerial Beach	187.3	488	49	0.14
22 May-4 June, 2001	Imperial Beach	Subaerial Beach	91.7	701	37	0.24-0.52
15-24 June, 2001	Solana Beach	Subaerial Beach	111.6	579	21	0.14
2-10 August, 2001	Cardiff	Subaerial Beach	77.2	274	46	0.34

[a]Placed in near-shore depths beneath the water surface.

[b]Placed south of the Tijuana River Mouth.

[*Coastal Frontiers Corporation*, 2002; *California Department of Boating and Waterways and State Coastal Conservancy*, 2002]

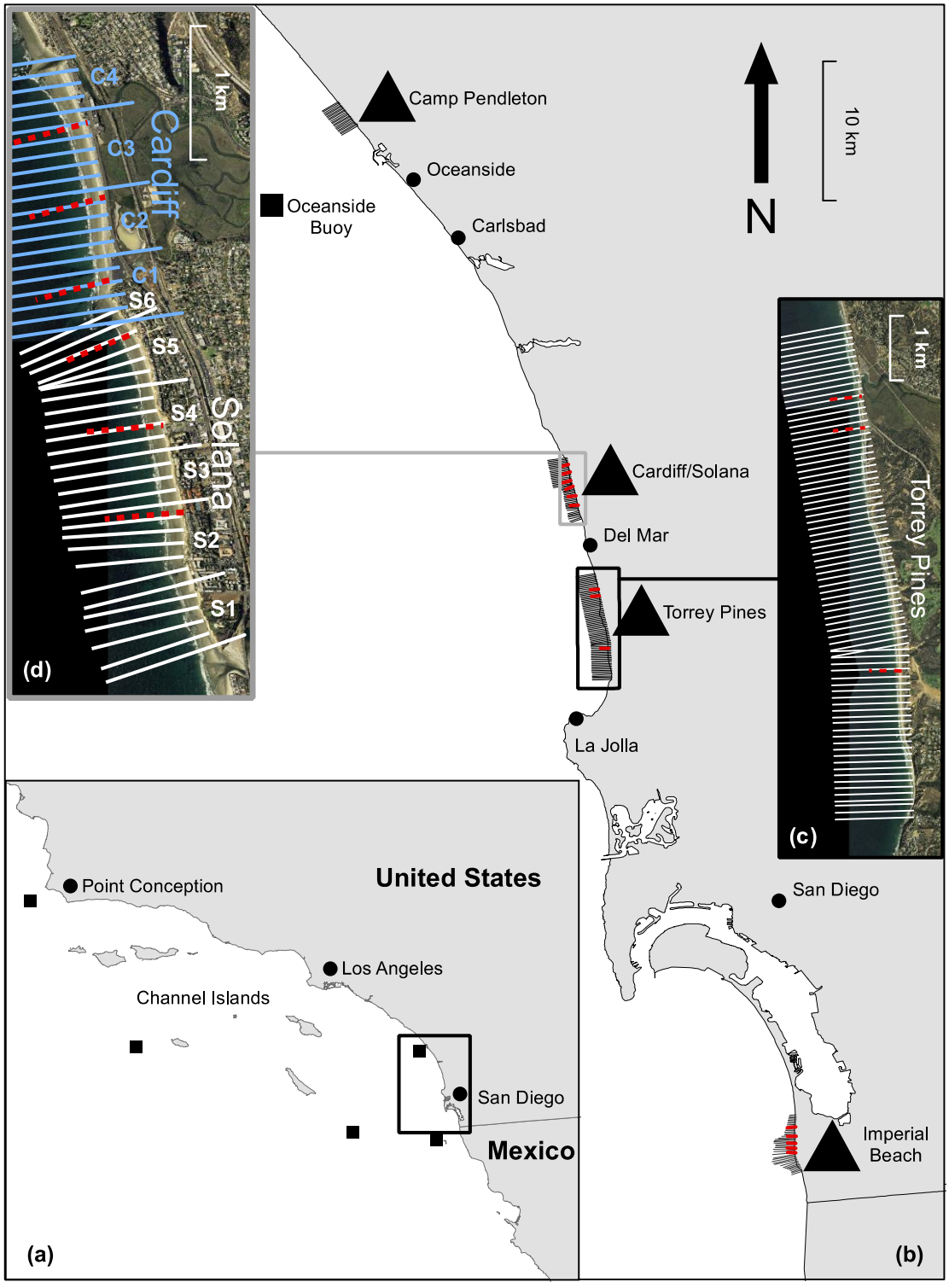
600 **Table 3.** Alongshore averages and standard deviations of optimal model free
601 parameters and R^2 at each site. Average characteristic adjustment timescales[a] $\tau^{\pm}$ are
602 shown in parenthesis and have units of days. The calibration period is October 2003-
603 October 2011. R^2 is for model runs over all available data.
604

	a_1 $(10^{-3}\,\mathrm{m}^2/\mathrm{m})$	C^- $(\mathrm{mh}^{-1}/\mathrm{m}^3)$	C^+ $(\mathrm{mh}^{-1}/\mathrm{m}^3)$	a_1C^- (τ^-) $(10^{-3}\ \mathrm{m}^{-1}\mathrm{h}^{-1})$	a_1C^+ (τ^+) $(10^{-3}\ \mathrm{m}^{-1}\mathrm{h}^{-1})$	R^2
Imperial Beach	-4.5±1.7	-0.92±0.72	-1.06±0.94	3.5±2.5 (21)	3.6±2.4 (64)	0.55±0.13
Torrey Pines	-2.2±0.9	-3.90±2.67	-4.58±2.02	6.6±3.2 (9)	10.3±5.7 (29)	0.58±0.08
Solana Beach	-5.8±2.5	-1.26±0.67	-0.83±0.43	7.6±3.5 (21)	4.0±1.7 (54)	0.60±0.08
Cardiff	-5.4±3.1	-2.16±1.52	-1.49±1.92	14.3±16.9 (14)	4.7±4.1 (57)	0.43±0.15
Camp Pendleton	-5.9±2.3	-0.62±0.10	-0.79±0.13	3.5±0.8 (12)	4.8±2.5 (41)	0.38±0.03

605 [a] $H_s = 4$ m (1 m) was used for estimating τ^- (τ^+).
606

607

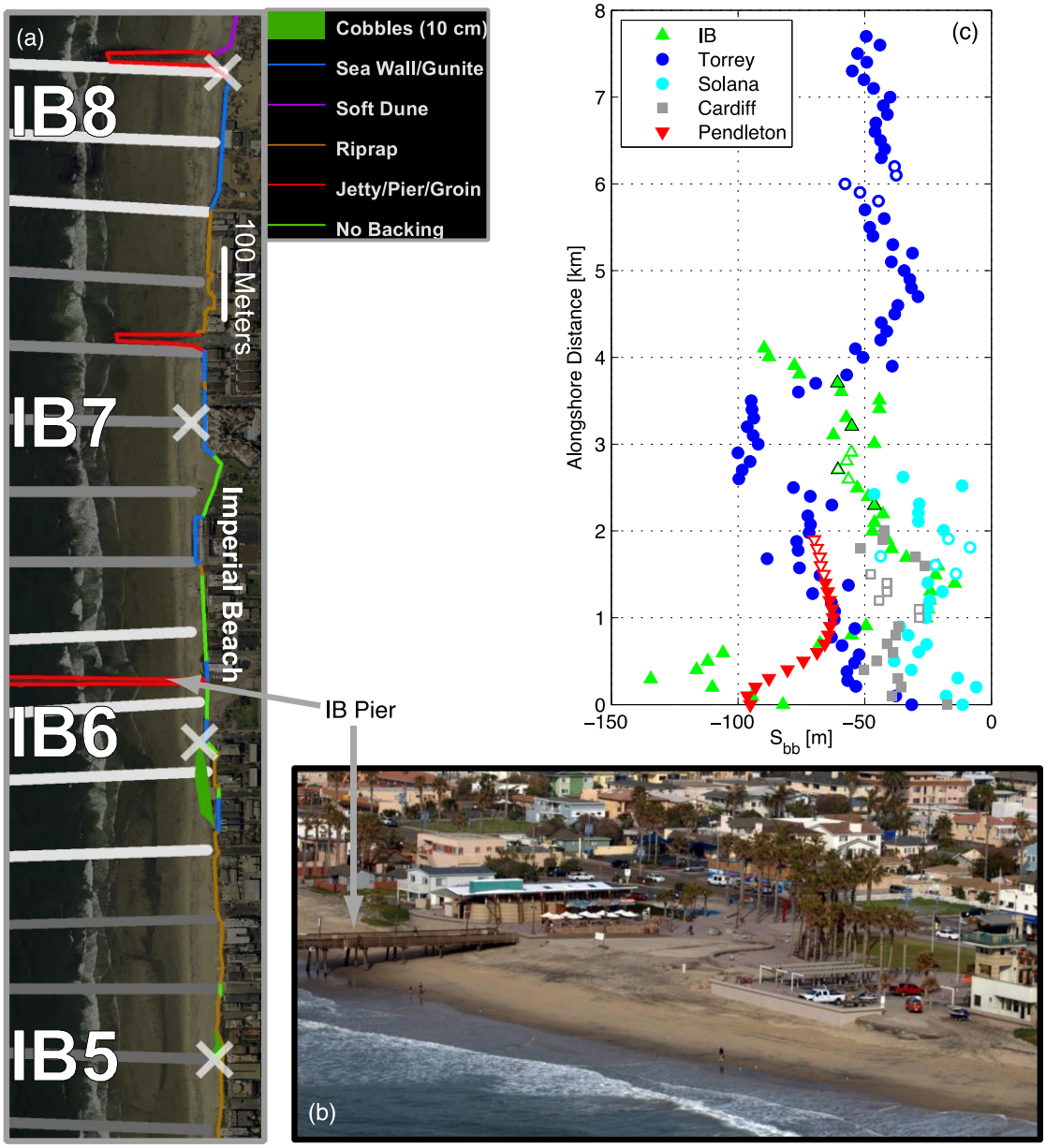
608 **Figures**



609

610

611 **Figure 1.** (a) Southern California map with wave buoy locations (black squares). (b)
612 San Diego area map with study beaches (black triangles), near-shore buoy (black square),
613 and survey transects (black (red) lines are SIO (SANDAG) transects). (c) Torrey Pines
614 and (d) Solana Beach and Cardiff plan views. Cross-shore transects of SIO quarterly
615 surveys (January, April, July, October) are white and blue lines, and SANDAG biannual
616 (May, October) are red lines. For model comparisons, surveys were alongshore averaged
617 in 500 m segments, labeled in (d).
618
619



620

621 **Figure 2.** (a) Aerial image of Imperial Beach with subaerial substrate and back beach

622 types (legend). Cross-shore survey transects, spaced 100 m alongshore, are averaged over

623 approximately 500 m alongshore sections for modeling (IB5-IB8; (a) centers marked

624 with white crosses). Transects within model section are indicated by alternating white

625 and gray transect shadowing (end sections have additional transects outside of frame

626 (a)). (b) Helicopter-based image of Imperial Beach (section IB6; February 2010).

Imperial Beach Pier in (a) and (b) is indicated with gray arrows. (c) The non-erodible shoreward boundary cross-shore location S_{bb} (referenced to the average shoreline (MSL) location; negative is shoreward) on each transect versus alongshore distance for all five beaches. $S_{bb} \approx$ -58 m for the heavily cobbled backbeach in section IB6 (alongshore distance 2.6-2.9 km). Location of 500 m modeled sections, for each beach in Figure 6, are indicated by markers with white centers in (c), and black edged triangles in (c) correspond to locations of transects nearest to white crosses in (a).

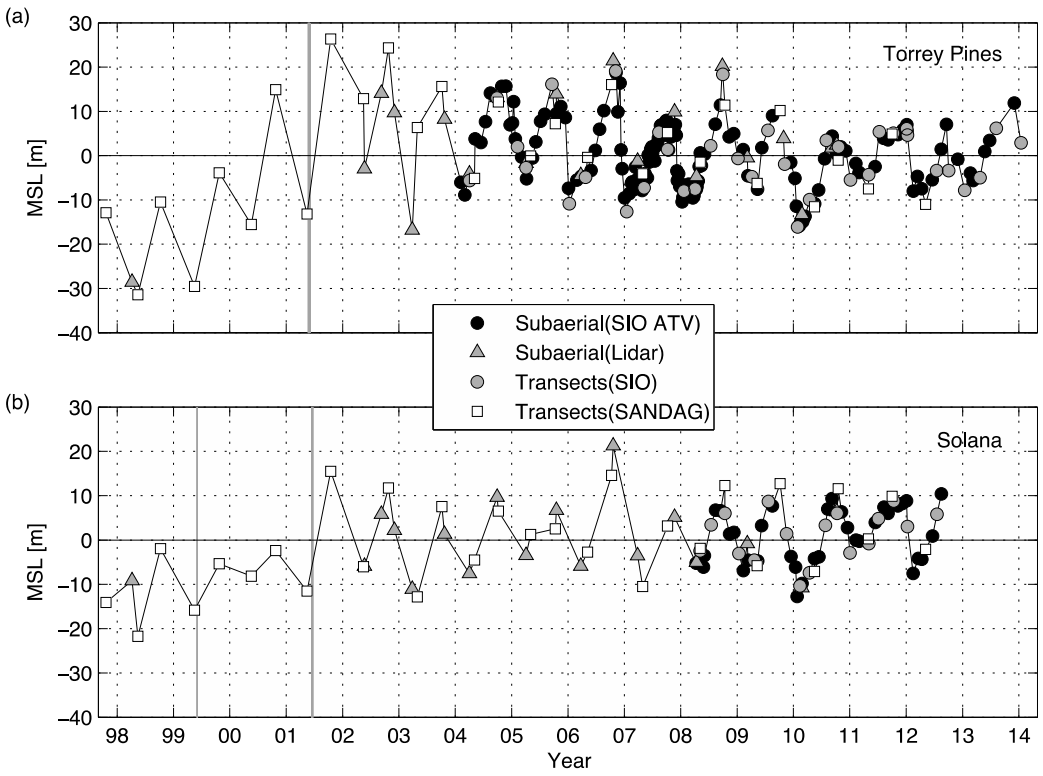


Figure 3. MSL cross-shore position (demeaned and alongshore averaged) versus time (tics are 1 January) for 16 years at (a) Torrey Pines and (b) Solana Beach. All available transects of each survey (legend indicates survey type, see Figure 1) are averaged. Positive (negative) values correspond to a wide (narrow) subaerial beach. Vertical gray lines indicate beach nourishment periods.

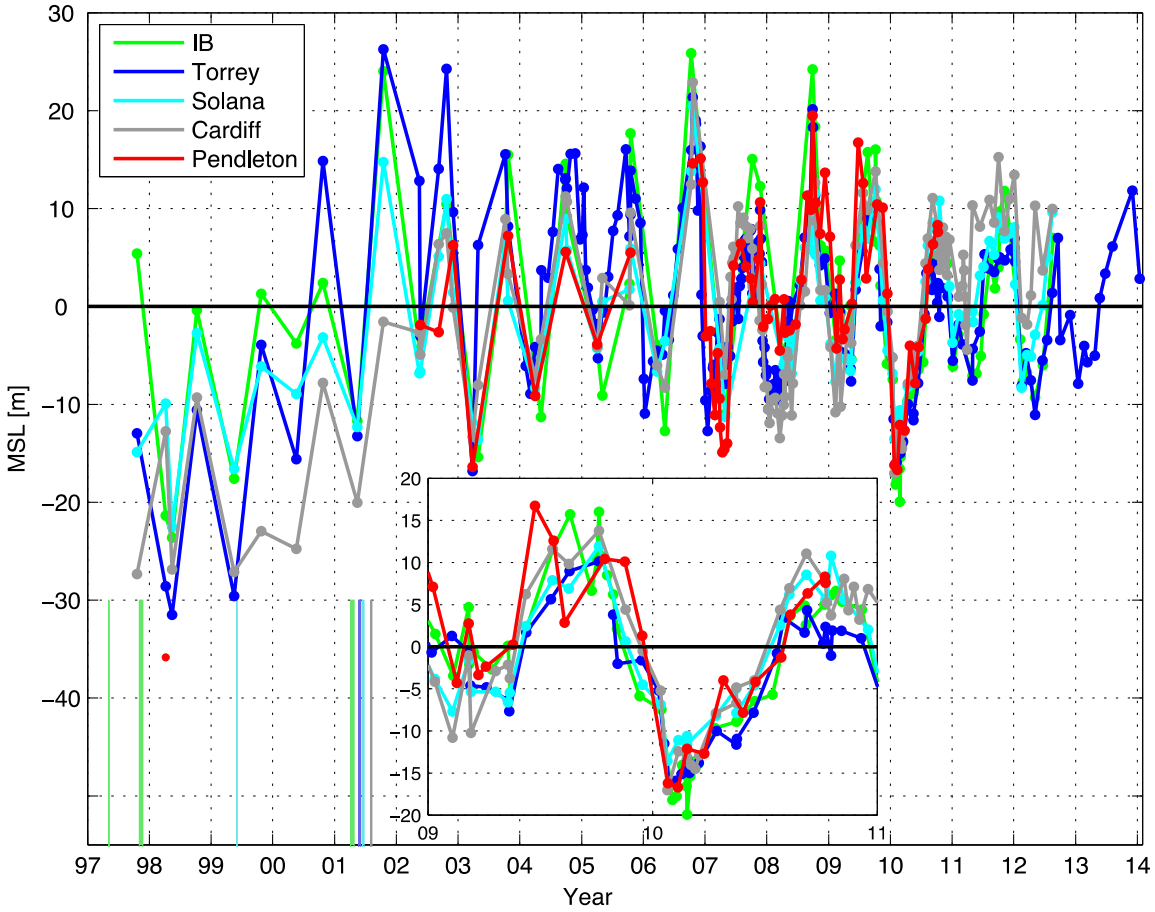
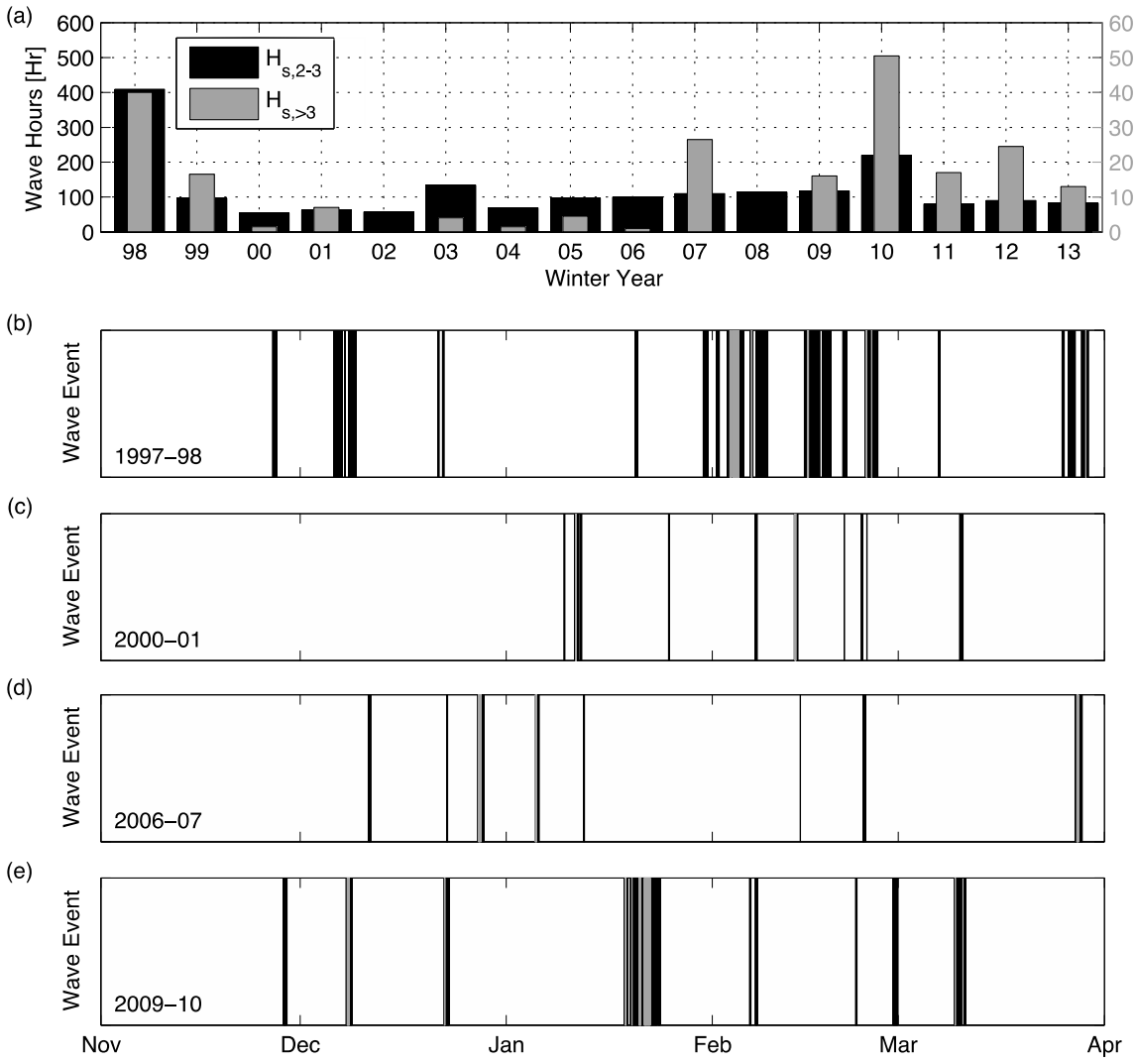


Figure 4. MSL cross-shore position (demeaned and alongshore averaged) versus time (tics are 1 January) for 16 years at 5 sites (see legend) from all data sources. Shortened colored vertical lines (see legend) indicate beach nourishment periods. Inset expands the 2009-10 El Niño winter.



669

670 **Figure 5.** (a) Hours of observed H_s between 2-3 m, and greater than 3 m (see legend)

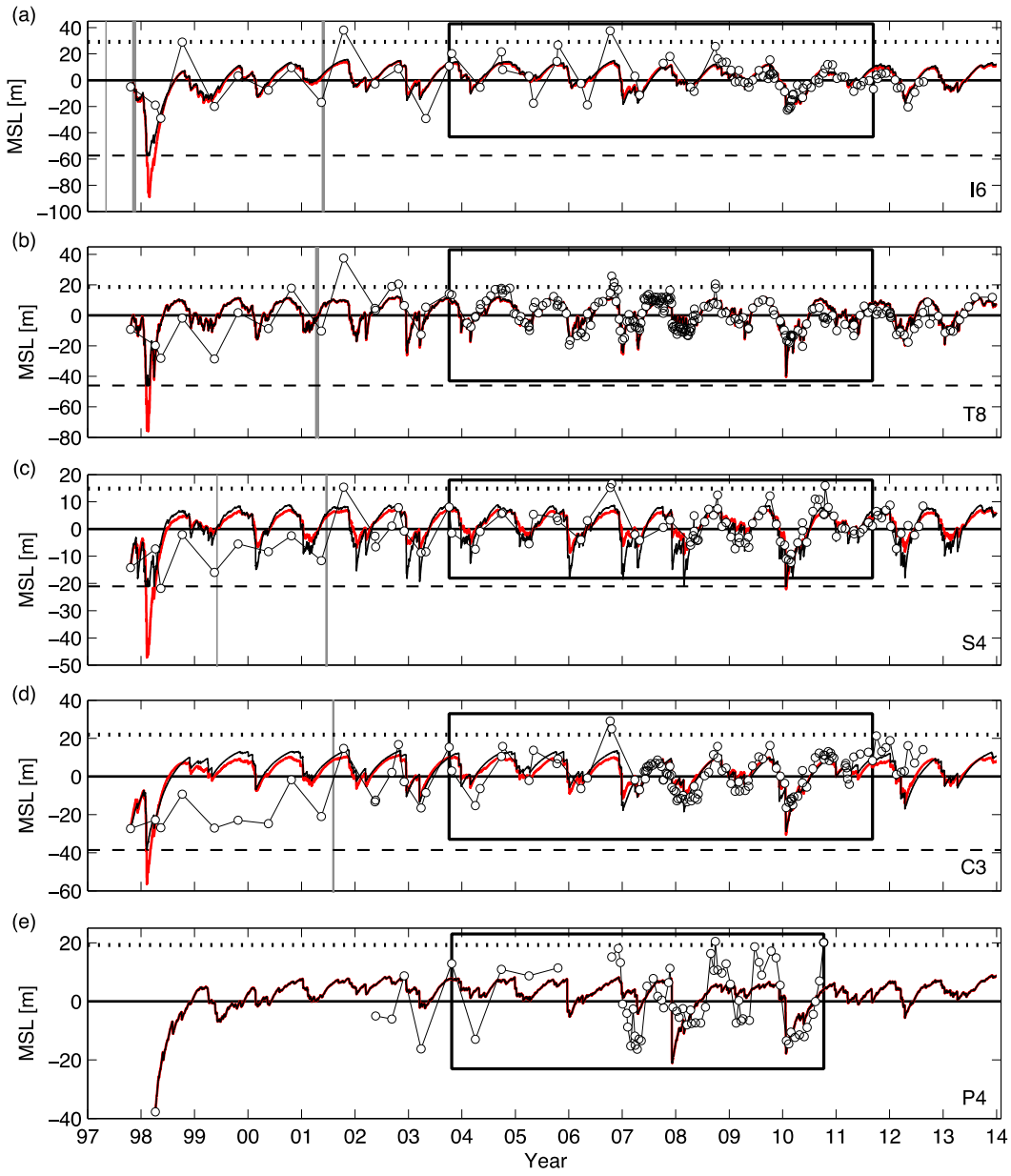
671 versus winter year (November-March) from November 1997 through March 2013 at

672 Oceanside Buoy (Figure 1). Temporal occurrences of wave events within H_s ranges

673 (legend) for winters (b) 1997-98 (El Niño), (c) 2000-01, (d) 2006-07, and (e) 2009-10 (El

674 Niño)

675



676

677 **Figure 6.** MSL position versus time (tics are 1 January) for representative 500 m long

678 sections at (a) Imperial Beach (section I6) and (b) Torrey Pines (T8), (c) Solana Beach

679 (S4), (d) Cardiff (C3), and (e) Camp Pendleton (P4). Shoreline observations are

680 white circles. Model predictions (linear$_4$ model, black curve; *Y09* model, red curve) differ

681 primarily in 1997-98. Model calibration period (black rectangle), non-erodible back

682 beach limit S_{bb} (dashed horizontal black line), fully equilibrated shoreline $S = -a_0/a_1$

683 for $E = 0$ (dotted horizontal black line), and beach nourishments (vertical gray bands)
684 are shown. Model root-mean-square errors (R^2) over 16-years are (a) 8.6 m (0.57), (b) 6.3
685 m (0.65), (c) 5.2 m (0.52), (d) 8.9 m (0.41), and (e) 8.8 m (0.43).
686
687
688
689
690
691
692
693
694
695
696
697
698

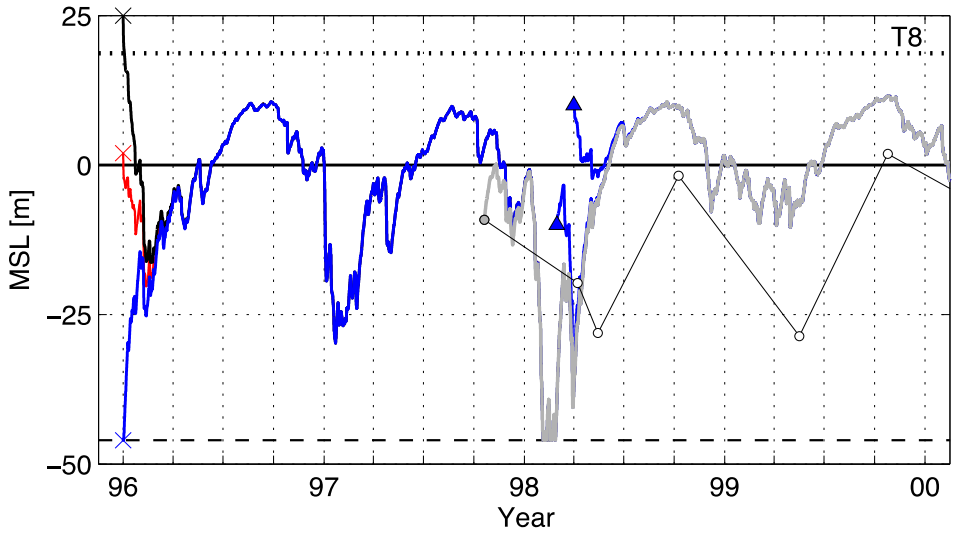


Figure 7. Modeled MSL position versus time at Torrey Pines (section T8, calibrated with 2003-2011 data) with different initial conditions. January 1996 with three hypothetical MSL shorelines (~0, 25 and -50 m; colored crosses) yield colored curves that rapidly converge together. Fall 1997 was initialized with the observed shoreline (gray circle and curve) and spring 1998 was initialized with ±10 m (two black-blue triangles). By summer 1998, all 6 model initializations yield the same result (gray curve). Horizontal lines are non-erodible back beach S_{bb} (dashed) and fully accreted beach (dotted), $S = -a_0/a_1$.

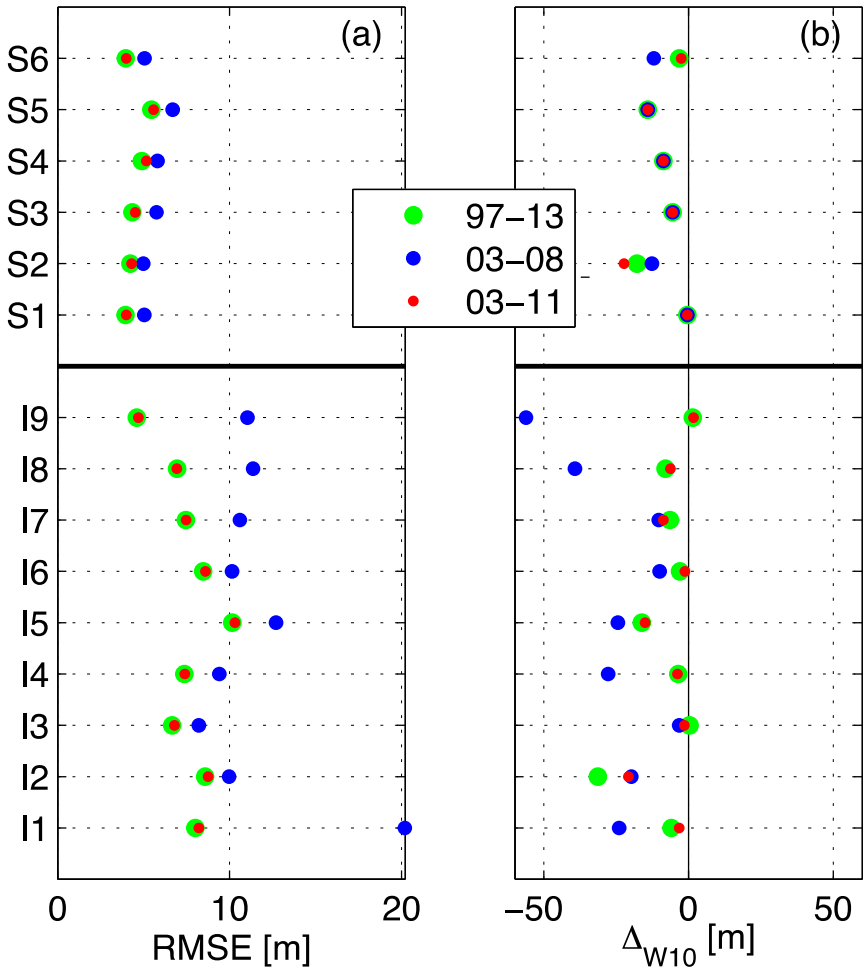


Figure 8. Model (linear$_4$) (a) RMSE (all data) and (b) model-data winter (January-March) 2010 erosion minimum error versus each 500 m alongshore section at Solana Beach (top, sections S1-S6) and Imperial Beach (bottom, I1-I9) for three model calibration periods. (b) Negative values indicate model over-predicts erosion minimum.

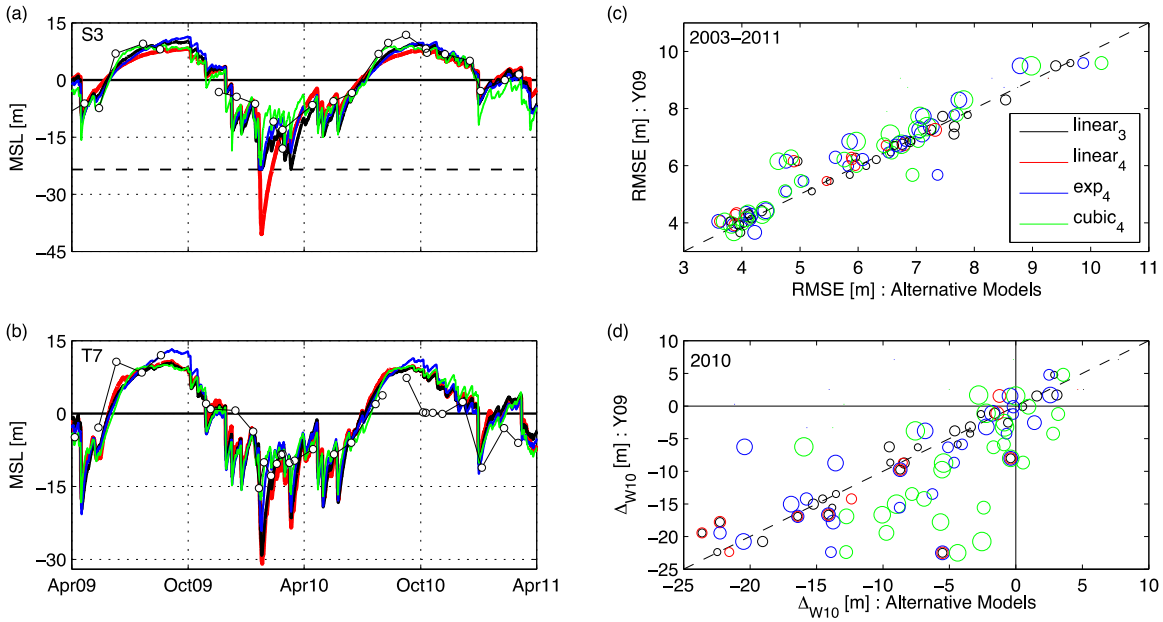
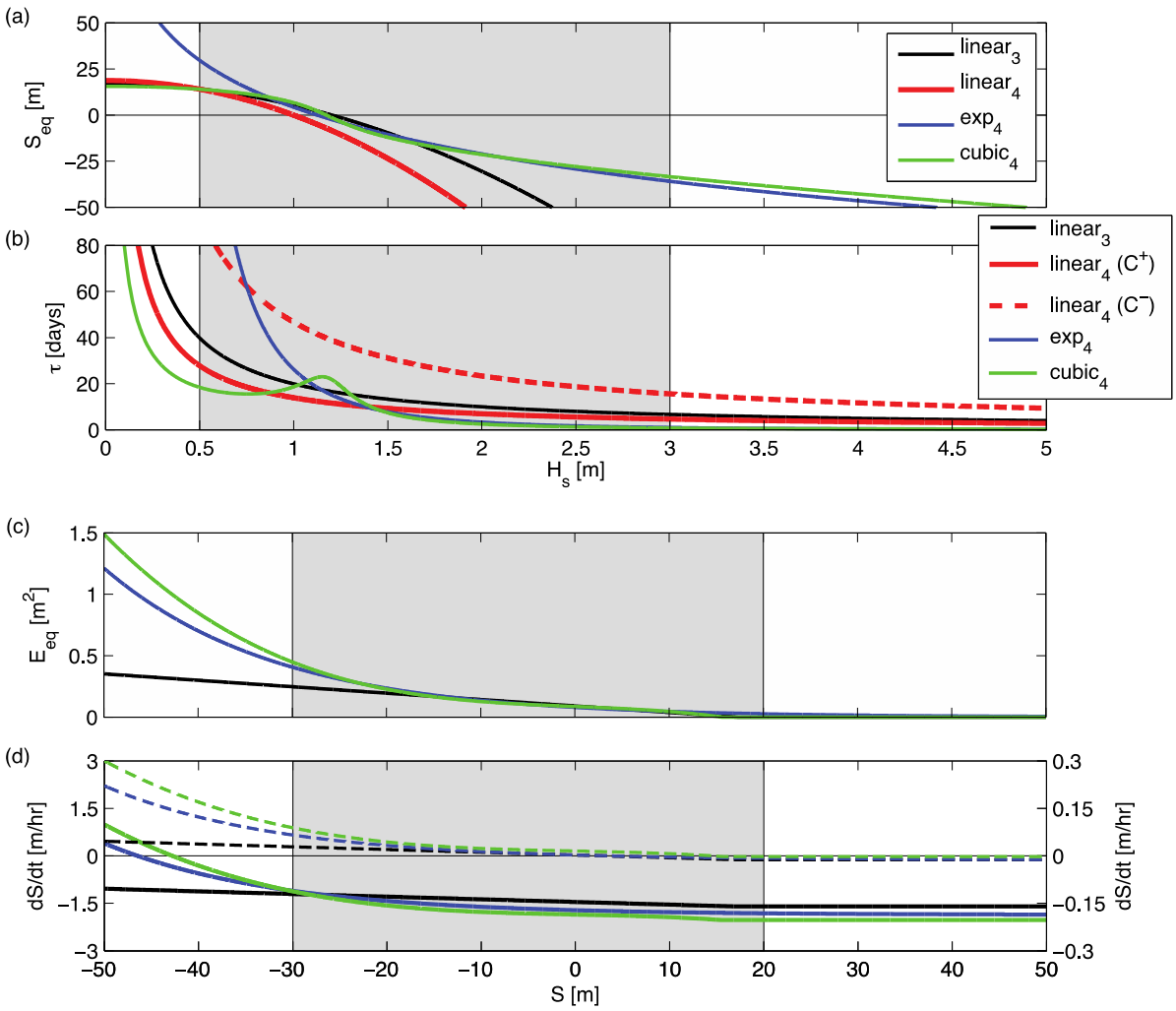


Figure 9. Modeled and observed (white circles) MSL versus time at (a) Solana Beach (section S3) and (b) Torrey Pines (T7). (a) Dashed black horizontal line indicates S_{bb}, the non-erodible back beach limit. Red curve in (a) and (b) is the *Yates et al.* [2009a] (unrestricted linear$_4$) model (e.g. *Y09* model). Note vertical scales differ in (a) and (b). (c) RMSE (October 2003-October 2011) and (d) model-data winter 2010 (January-March 2010) erosion minimum error for the *Y09* model (vertical axis) versus alternative models. In panels (c) and (d), symbol size varies for visibility. (a-d) Model types are indicated by colors (legend in (c)).



743

744 **Figure 10.** Example model results for Torrey Pines section T8 parameters: (a)

745 equilibrium shoreline position S_{eq}, and (b) characteristic response time scale τ, both

746 versus significant wave height H_s. See legend for model types. (c) Model E_{eq} and (d)

747 shoreline change rate dS/dt, both versus shoreline position S. An accreted beach has

748 $S > 0$ and an accreting beach has $dS/dt > 0$. In (d), results are shown for high (H_s = 4 m;

749 solid curves; left vertical axis) and low (H_s = 0.4 m; dashed curves; right vertical axis)

750 energy waves. Shading indicates the range of commonly occurring H_s and S.

751